Adherend thickness effect on the tensile fracture toughness of a structural adhesive using an optical data acquisition method

R.D.S.G. Campilho[a,b,n], D.C. Moura[c,d], M.D. Banea[c], L.F.M. da Silva[c]

[a] *Departamento de Engenharia Mecânica, Instituto Superior de Engenharia do Porto, Instituto Politécnico do Porto, Rua Dr. António Bernardino de Almeida, 431, 4200-072 Porto, Portugal*

[b] *Faculdade de Ciências Económicas, Sociais e da Empresa, Universidade Lusófona do Porto, Rua Augusto Rosa, 24, 4000-098 Porto, Portugal*

[c] *Faculdade de Engenharia da Universidade do Porto, Rua Dr. Roberto Frias, s/n, 4200-465 Porto, Portugal*

[d] *INEGI—Instituto de Engenharia Mecânica e Gestão Industrial, Rua Dr. Roberto Frias, 400, 4200-465 Porto, Portugal*

ABSTRACT

Adhesive bonding is nowadays a serious candidate to replace methods such as fastening or riveting, because of attractive mechanical properties. As a result, adhesives are being increasingly used in industries such as the automotive, aerospace and construction. Thus, it is highly important to predict the strength of bonded joints to assess the feasibility of joining during the fabrication process of components (e.g. due to complex geometries) or for repairing purposes. This work studies the tensile behaviour of adhesive joints between aluminium adherends considering different values of adherend thickness (*h*) and the double-cantilever beam (DCB) test. The experimental work consists of the definition of the tensile fracture toughness (*G*IC) for the different joint configurations. A conventional fracture character- ization method was used, together with a *J*-integral approach, that take into account the plasticity effects occurring in the adhesive layer. An optical measurement method is used for the evaluation of crack tip opening and adherends rotation at the crack tip during the test, supported by a Matlab® sub-routine for the automated extraction of these quantities. As output of this work, a comparative evaluation between bonded systems with different values of adherend thickness is carried out and complete fracture data is provided in tension for the subsequent strength prediction of joints with identical conditions.

Keywords:
Aluminium and alloys Experimental testing Joint design, Fracture

1. Introduction

In order to increase the efficiency of structures and reduce their weight, adhesively-bonded joints can be used over fastening, riveting or other traditional joining methods. Different joint configurations can be applied in structures, such as single-lap, double-lap, stepped and scarf. Many other configurations exist, with specific advantages, like the joggle-lap joints, applied for instance to join fuselage parts in aircraft, reinforcement doublers, peel joints and L-section joints. Adhesives are progressively being applied in structures of several branches of engineering, which also makes certification-related issues more important, especially in industries such as aeronautics [1]. Because of this, it is highly important the availability of robust predictive techniques that can reliably be used as design tools, to allow minimization of experi- mentation during the design stages of products and structures without compromising the design process [2,3]. This will allow assessing the feasibility of joining during the fabrication process of components (e.g. due to complex geometries) or joining as a repair method. A large number of predictive techniques are currently available, ranging from analytical to numerical, using different criteria to infer the onset of material degradation, damage or even complete failure. Initially, the prediction was performed by theo- retical studies as those of Volkersen [4] or Goland and Reissner [5], which had a lot of embedded simplifying assumptions, by compar- ing current stresses with the allowable material strengths. Many improvements were then introduced, such as the assumption of elasto-perfectly plastic adhesive proposed by Hart-Smith [6], but these analyses usually suffered from the non-consideration of the material ductility, which is highly relevant because of stress gradients. Fracture mechanics-based methods took the fracture toughness of materials as the leading parameter for material selection. These methods included more simple energetic or stress-intensity fracture techniques that required the existence of an initial flaw in the materials [7]. More recent numerical techniques, such as cohesive zone models (CZM), combine stress criteria to account for damage initiation with energetic, e.g. fracture toughness, data to estimate damage propagation [8]. This allows to consider the distinct ductility of adhesives and to gain

accuracy in the predictions. All of these fracture toughness- dependent analyses rely on an accurate measurement of G_{IC} and G_{IIC} (shear toughness). CZM in particular can accurately predict damage growth in structures if the fracture laws are correctly estimated [9]. These fracture laws are based on the values of cohesive strength in tension and shear, t_n^0 and t_s^0, respectively, and also G_{IC} and G_{IIC} [10]. These parameters that cannot be directly related with the material properties measured as bulk, since they account for constraint effects (in the case of adhesive joints, the constraints are caused by the adherends). Although these para- meters do not have a clear physical significance, they are able to accurately reproduce the behaviour of the materials in a macro scale point of view that is quite accurate [2]. The estimation of these fracture parameters is generally accomplished by perform-ing pure tension or shear tests. Regarding G_{IC}, the DCB test is the most suitable, due to the test simplicity and accuracy [11]. The typical G_{IC} estimation methods are based on linear-elastic fracture mechanics (LEFM) and require the continuous measurement of the crack length (a) during the test. However, G_{IC} of adhesives with large scale plasticity is not accurately characterized with LEFM methods since the assumed stress fields at the crack tip vicinity are not accurate [12]. More recently, methods that do not requirethe measurement of a were developed, based on equivalent cracks and including the plasticity effects around the crack tip [13]. As it was described by Suo et al. [14], in the presence of large-scale plasticity, J-integral solutions can also be employed for accurate results. The J-integral is a relatively straight-forward technique, provided that the analytical solution for a given test specimen exists for the determination of G_{IC} or G_{IIC}. The most prominent example is the DCB specimen, for which J-integral solutions are available, either for loading by pure bending moments [15] or the standardized and moment-free tensile loading [16]. It is also possible to estimate the tensile CZM law. Carlberger and Stigh [17] computed the CZM laws of adhesive layers in tension and shear using the DCB and end-notched flexure (ENF) tests, respec- tively, considering $0.1 \leq t_A \leq 1.6$ mm (t_A is the adhesive thickness). The rotation of the adherends was measured by an incremental shaft encoder and the crack tip opening by two linear variable differential transducers (LVDT). Ji et al. [18] studied the influence of t_A in DCB joints on t_n and G_{IC} for a brittle epoxy adhesive. G_{IC} was measured by a direct technique. For the measurement of the adherends rotation, two digital inclinometers with a 0.011 precision were attached at the free end of each adherend. The normal displacement at the crack tip was measured by a charge- coupled device (CCD)camera.

Regarding the fracture parameters of adhesives, different studies showed that these are similar as bulk and in a joint for brittle adhesives, since the yield zone ahead the crack tip is practically nonexistent [19]. Contrarily, when speaking about moderately-to-highly ductile adhesives, the fracture parameters are not invariant to the joint geometry [20,21]. This occurs because of the different degree of restriction to the development of this yield zone within the adhesive layer and also premature adhesive fracture because of excessive adherend yielding near the adhesive layer. This brings issues about the transfer of small specimen (test) results to real-life and complex structures. Actually, the majority of industrial structures bonded by adhesives consist of thin sheets between 1 and 3 mm thick, whilst the fracture behaviour of adhesives is mostly characterized within considerably thicker joints [22]. Pardoen et al. [23] discussed the two types of constraint effects that affect the fracture toughness of adhesive layers in bonded assemblies: external and internal constraint effects. External effects deal with the varying states of deformation of the adherends, which alter the stress and strain distributions of the adhesive layer. For instance, Wang et al. [24] found that G_{IC} of adhesives measured in peel tests varies upon the thickness of the peeling arms. Internal constraint effects are t_A and specimen width(B), which also influence the size of the yield zone and stress andstrain distributions in the adhesive. As an example, the increase of t_A can change the yielding conditions from small-scale to fullplastic [25]. In the work of Giannis et al. [26], two different sealants for aircraft fuel tanks were tested by a modified peel test,and it was shown for both adhesives that t_A largely increasedthe peel resistance between 2 and 4 mm. Because of these issues,taking into account of these constraints requires a precise simula-tion of the states of deformation of both the adhesive andsurrounding structure. One of the methods that allow this to bemodelled is CZM, by considering the adhesive layer modelled bycohesive elements [27].

Most of the published work addressing the influence of h examines directly its influence on the failure loads, either static [28] or fatigue [29] and, in general, increasing h has shown to improve the strength. Some studies associated this behaviour to the reduction of peel and shear peak stress at the overlap edges of bonded structures [30]. This actually occurs, but other phenomena are also on the basis of these differences in strength. Actually, a few studied showed variations of G_{IC} by modification of the structures thickness. In the work of Mangalgiri et al. [31], sym- metric and unsymmetric DCB specimens were experimentally tested with different values of h (by considering 8, 16 or 24 plies of carbon–fibre adherends). The static tests showed a large improvement of G_{IC} between composites with 8 and 16 plies. Devitt et al. [32] equally used the DCB test to investigate this effect, and found a 9% increase in the value of G_{IC} of bonded joints made of glass-epoxy composites by duplicating the number of plies of the adherends. From these studies, it is clear that the differences take place at relatively low h values. Since most bonded joints are made between thin adherends/sheets, the understanding of how h affects the fracture toughness is highly relevant.

In this work, the value of G_{IC} of adhesive joints between aluminium adherends is studied, considering different values of$h$ and the DCB test. A conventional fracture characterization method was used, in comparison with a J-integral approach, thattake into account for the plasticity effects occurring in the adhesive layer. An optical measurement method is used for the evaluation of crack tip opening and adherends rotation at the crack tip during the test, supported by a Matlab® sub-routine for the automated extraction of these quantities.

2. Experimental work

2.1. Characterization of the materials

The adherends were cut from a high strength aluminium alloy sheet (AA6082 T651) by precision disc cutting. This material was characterized in bulk tension in previous works by the authors [33,34] using dogbone specimens and the following mechanical properties were obtained: Young's modulus (E) of 70.07 ± 0.83 GPa, tensile yield stress (σ_y) of 261.67 ± 7.65 MPa, tensile failure strength (σ_f) of 324 ± 70.16 MPa and tensile failure strain (ε_f) of 21.70 ± 4.24%. The two-component polyurethane adhesive SikaForce® 7888, selected for this work, was formerly tested in the work of Neto et al. [35]. The bulk specimens were tested in a servo-hydraulic machine to obtain E, σ_f and ε_f. The DCB test was selected to obtain G_{IC} and the ENF test was used for G_{IIC}. The collected data of the adhesive is summarized in Table 1. To be noted that the obtained values of G_{IC} and G_{IIC} were obtained in partial adhesive failure conditions, which is important to notice when comparing G_{IC} with the results obtained in this work.

Table 1
Properties of the adhesive SikaForce® 7888 [35].

Property	
Young's modulus, E [GPa]	1.89 ± 0.81
Tensile yield strength, σ_y [MPa]	13.20 ± 4.83
Tensile failure strength, σ_f [MPa]	28.60 ± 2.0
Tensile failure strain, ε_f [%]	43.07 ± 0.6
Critical energy release rate in tension, G_{IC} [N/mm]	0.70 ± 23
Critical energy release rate in shear, G_{IIC} [N/mm]	8.72

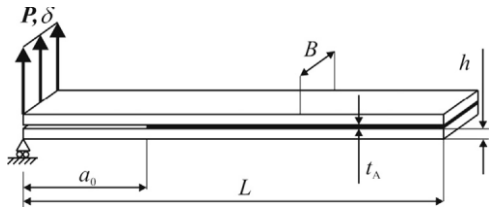

Fig. 1. Geometry of the DCB specimens.

2.2. Joint geometries

Fig. 1 represents the geometry of the DCB specimens. The dimensions of the specimens are: total length L = 160 mm, initial crack length a_0 ≈ 40 mm, h = 1, 2, 3 or 4 mm, B = 25 mm and t_A = 1 mm. The bonding process consisted in grit blasting with corundum sand, debris cleaning with acetone and assembly in a steel mould for the correct alignment between the adherends. To guarantee a uniform t_A value, calibrated spacers were inserted between the adherends. The required sharp pre-crack was assured using a 0.1 mm thick razor blade between calibrated bars at the crack tip. After applying the adhesive and assembling the speci- mens, these were given a full cure before testing. The spacers were removed and the adherends sides were sprayed with white brittle paint, to allow an easy identification of a, and a printed scale was glued in both adherends to aid the a measurement or input data for the digital correlation technique. Twenty-four specimens were tested (six for each configuration) at room temperature and 1 mm/min in an electro-mechanical testing machine (Shimadzu AG-X 100) with a load cell of 100 kN. Each test was fully documented using a 18 MPixel digital camera with no zoom and fixed focal distance to approximately 100 mm. This procedure allowed obtaining the crack tip opening (δ_n) and rotation (θ_o), necessary for the J-integral method. The correlation of the mentioned parameters with the load–displacement (P–δ) data was done by the time elapsed since the beginning of each test.

3. Estimation of G_{IC}

It is known that, when the adhesives are ductile, as it occurs with the Sikaforce® 7888, LEFM methods are inaccurate [36], even though considering techniques with correction factors to account for plasticity (e.g. ASTM D3433-99:2005 and BS 7991:2001). Thus, the compliance-based beam method (CBBM), which accounts for the damage zone ahead of the crack tip, and the J-integral, were considered for the present study.

3.1. Compliance-based beam method

The CBBM was initially selected to measure G_{IC} of the adhesive [13]. It is a relatively straightforward but robust method, based on an equivalent crack, and it only depends on the specimen's compliance during the test. Applied to the DCB test specimen, it gives

$$G_{IC} = \frac{6P^2}{B^2 h}\left(\frac{2a_{eq}^2}{h^2}\frac{E_f}{5G} + \frac{1}{5}\right) \quad (1)$$

While detailed explanations are presented elsewhere [13], a brief explanation of the parameters is given: a_{eq} is an equivalent crack length estimated from the current specimen compliance and taking into consideration the damage zone, E_f is a corrected flexural modulus to account for phenomena affecting the P–δ curve, such as stress concentrations at the crack tip and stiffness variability between specimens, and G is the shear modulus of the adherends [37].

3.2. Direct method to define G_{IC} and the CZM law

The method followed in this work allows obtaining the cohe- sive law of the adhesive by the simultaneous measurement of the J-integral and δ_n [16]. The J-integral applies to the non-linear elastic behaviour of materials, but it remains valid in the presence of a plastic but monotonically-applied loading, as it is the case of the cohesive separation and plastic dissipation in adhesive layers [18]. Based on the fundamental expression for J defined by Rice[38], it is possible to present a closed-form solution for the tensileenergy release rate (G_I) from the concept of energetic force andalso the beam theory for the DCB specimen, as [39]:

$$G_I = 12\frac{P_u a^2}{E_a h^3}P_u\theta_o \quad (2)$$

or

$$G_I = P_u\theta_p; \quad (3)$$

where P_u represents the applied load per unit width at the adherends edges, E_a the Young's modulus of the adherends and θ_p the relative rotation of the adherends at the loading line (Fig. 2). Expression (2) was used in the present work, considering θ_o instead of θ_p, to gain accuracy in the measurements, since the optical method is inherently more precise. The J-integral is defined along an arbitrary path encircling the start of the adhesive layer, giving [18]:

$$G_n = \int_0^{\delta_{nc}} t_n(\delta_n)\,d\delta_n: \quad (4)$$

The value of δ_{nc} corresponds to the crack-tip end-opening at failure of the cohesive law, while t_n is the current normal traction. G_{IC} is the value of G_I when the crack initiates propagation, and is given by the steady-state value of G_I in the G_I–δ_n plot [18]. The $t_n(\delta_n)$ plot is obtained by differentiation of Eqs. (2) and (3) with respect to δ_n

$$t_n(\delta_n) = \frac{\partial G_I}{\partial \delta_n} \quad (5)$$

3.2.1. Optical method for the parameter measurement

The process detailed here is an improvement of the work developed by the authors in reference [40]. For calculating δ_n and θ_o for a given image, the optical method requires the identification of eight points (Fig. 3): two points (p_3 and p_4) for measuring the current t_A value at the crack tip (t^{CT}) during loading in image units (pixels), two points (p_7 and p_8) identifying a line segment in the image for which the length (d) is known in real world units (mm), two points (p_1 and p_5) on the top specimen and two points (p_2 and p_6) on the bottom specimen for computing θ_o.

3.2.1.1. Points identification. All eight points are manually identified in the first picture of a trial using an in-house software tool. The

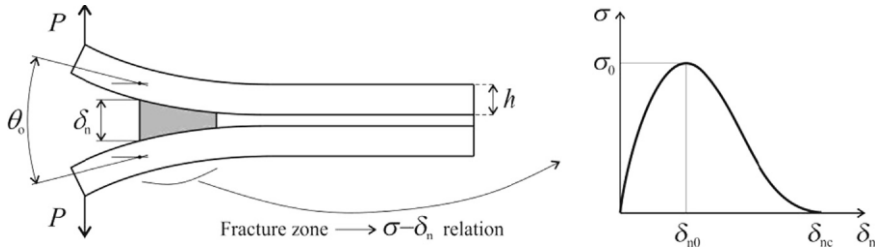

Fig. 2. DCB specimen under loading, with description of the analysis parameters.

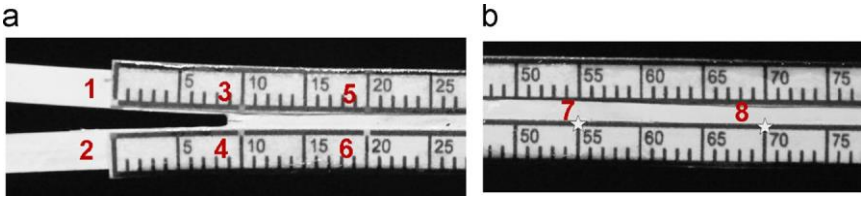

Fig. 3. Points taken by the optical method to measure δ_n and θ_o.

identification of the points is aided by the ruler attached to the specimens, which helps finding their correct locations. In addition, each point between p_1 and p_6 is printed with a distinct colour (although this is not perceptible in Fig. 3). Using the location of the points in the first picture, the points of the following pictures are automatically identified using a computer algorithm implemented in Matlab®. Basically, for each point p_i, a rectangular region centred in p_i is extracted from the first image forming a template (t). This template describes the image pattern that surrounds the point and is used for locating the point in the next image. This is done by finding the position (u,v) in the next image (I) that has the highest normalized cross-correlation with the template. The normalized cross-correlation is a measure of similarity between two images that is invariant to linear changes in the pixel intensities and that quantifies the correlation between two images/regions [41]. This measure of similarity was chosen due to its low computational requirements, which is a critical factor given the high resolution of the images, and because changes in rotation and scale of the specimens are expected to be small between two consecutive acquisitions (gapped by 5 s). To take advantage of the colour information, the colour space of the images (and consequently, of the templates) was transformed to the CIELAB colour space. The CIELAB system represents the value of a pixel by three components, L, a and b, where L represents luminosity and a and b define colour. Since points p_1 to p_6 are differentiated by their colour, only the a and b components are used when detecting points. The normalized cross-correlation (γ) of template t with image I at the position (u,v) of image I for the colour component c is defined as:

$$\gamma(u,v;c) = \frac{\sum_{x,y}[I(x,y;c)-\bar{I}_{u,v;c}]\times[t(x-u,y-v;c)-\bar{t}_c]}{\left\{\sum_{x,y}[I(x,y;c)-\bar{I}_{u,v;c}]^2\times\sum_{x,y}[t(x-u,y-v;c)-\bar{t}_c]^2\right\}^{0.5}} \quad (6)$$

where $I(x,y,c)$ is the intensity of the colour component c of the pixel (x, y) of image I; $t(x,y,c)$ is the intensity of the colour component c of the pixel (x,y) of the template t; $\bar{I}_{u,v;c}$ is the average intensity of the colour component c of the region of image I centred at pixel (u,v) and with the same size as t, and $\bar{t}_c$ is the average intensity of the colour component c for the template t. Finally, the normalized cross- correlation for a single pixel taking into account the colour components a and b is defined as:

$$\gamma(u,v) = \sqrt{\gamma(u,v,a)^2+\gamma(u,v,b)^2}. \quad (7)$$

Calculating γ for all the pixels of I results in a matrix where the maximum absolute value yields the location of the region in I thathas the highest correlation with t and, thus, the most likely location of p_i in the next image. This is done for every one of theeight points identified in the first image. After successfully identifying all the points of the second image, new templates arecomputed from the second image to search for the eight points inthe third image, and so on until processing all images.

3.2.1.2. Computation of δ_n. The value of t_A^{CT} in real world units (mm) is calculated as follows

$$t_A^{CT} = d\,\frac{p_4-p_3}{\overline{p_7-p_8}}; \quad (8)$$

Assuming that the lens distortion is negligible, which is valid for the central area of pictures acquired with modern CCD cameras [42]. A length of d = 15 mm was used for all trials (illustrated in Fig. 3). The pixel size was on average 0.021 mm and, thus, the estimated maximum error of the image acquisition process is 0.011 mm. Finally, δ_n can be defined as

$$\delta_n = t_A^{CT} - t_A; \quad (9)$$

where t_A is the theoretical design value of 1 mm. Since t_A can showsmall variations due to the fabrication process, an adjustment to δ_n is also applied to make δ_n = 0 at the beginning of the test (detailedin Section 4).

3.2.1.3. Computation of θ_o. θ_o is calculated as the angle between the tangents to the horizontal curves of the 2 scales closest to the adhesive, measured at the crack tip (Fig. 4). The curvature of the top adherend is first computed by fitting a quadratic function to points p_1, p_3 and p_5. The first derivative of the quadratic function at p_3 yields the slope of the top curve (m_{top}) at the crack tip, which is then used to define a direction vector $\vec{v}_{top} = (1, m_{top})$. The same process is repeated for points p_2, p_4 and p_6, yielding the slope of the tangent to the bottom curve at the crack tip (m_{bottom}) and its direction vector $\vec{v}_{bottom} = (1, m_{bottom})$. Finally, θ_o is obtained by measuring the angle between the two vectors:

$$\theta_o = \arccos\left(\frac{\vec{v}_{top}\times\vec{v}_{bottom}}{\|\vec{v}_{top}\|\,\|\vec{v}_{bottom}\|}\right). \quad (10)$$

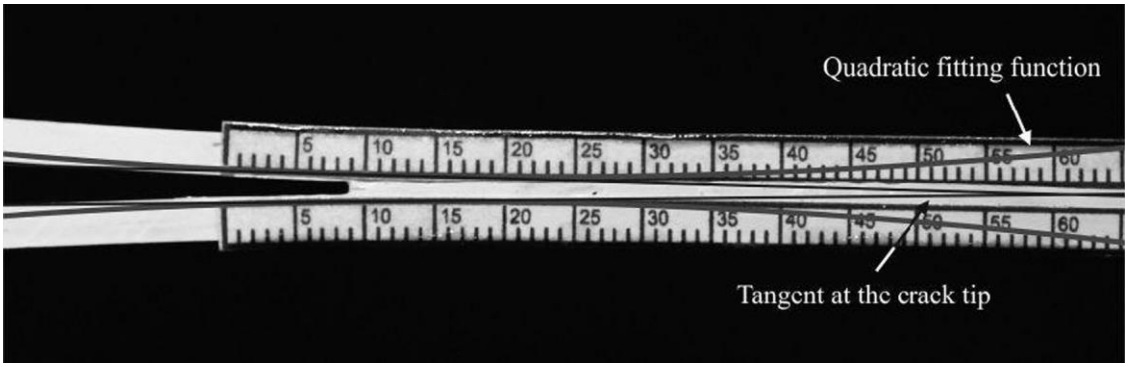

Fig. 4. Calculation of θ_O. Quadratic functions were fitted to points $p1$, $p3$, $p5$ and $p2$, $p4$, $p6$, representing the curvature of the top and bottom specimen, respectively, while the straight lines show the tangents to the curves at the crack tip (corresponding to 10 mm in the scales).

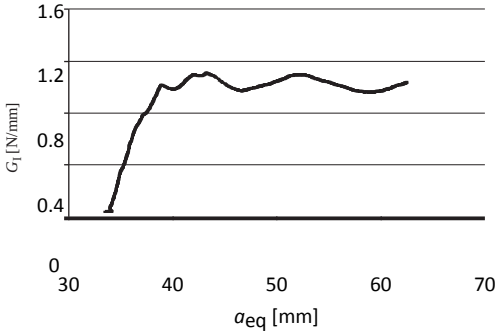

Fig. 5. Evolution of G_I with a_{eq} for a test specimen with h ¼ 3 mm.

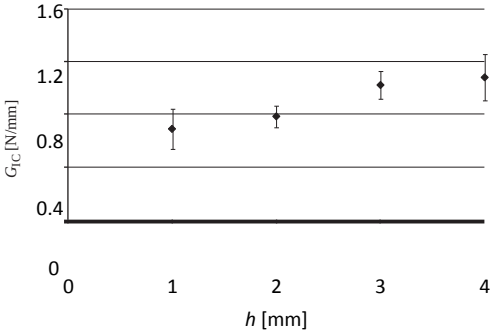

Fig. 6. Average values and deviation of G_{IC} as a function of h by the CBBM.

4. Results

After having performed the tests on the DCB specimens with varying values of t_A, no signs of plasticity were found in the adherends, although for the specimens with t_A ¼1 mm the tensile displacements of the loading points during crack propagation was significant.

4.1. Evaluation of G_{IC} by the CBBM

G_{IC} was initially estimated by the CBBM, which is a well known method for this purpose, and allows accounting for the plasticity of materials. By using this method, it was possible to obtain the R-curve for each specimen, relating G_I with a_{eq}, as the crack progressed. Fig. 5 gives an example of an experimental R-curve obtained by this technique for a specimen with h ¼ 3 mm, clearly showing the attainment of a steady-state value of G_I. For this specimen, a_0 was measured at 31.50 mm. The corresponding value of a_{eq} by the CBBM was 38.57 mm, calculated directly from the P–δ data by the first drop of P in the P–δ curve. This difference occurred since a_{eq} accounts for the damage zone [13]. Fig. 6 compares the G_{IC} (N/mm) values of the specimens with varying values of h, including the standard deviation for each batch of specimens. An increasing trend for G_{IC} was found as a function of h, starting from the specimens with h ¼ 1 mm, with a steeper increase up to 3 mm and stabilization above this value. Fig. 6 also shows some deviation between specimens of identical conditions, but perfectly within reported deviations under identical testing conditions [40]. Actually, this scatter is related to experimental phenomena such as fabrication issues or small measurement errors or geometry deviations. However, the reliability of the observed tendency with h obviously cannot be questioned, or solely attributed to experimental scatter, on account of the large improvement visible in Fig.

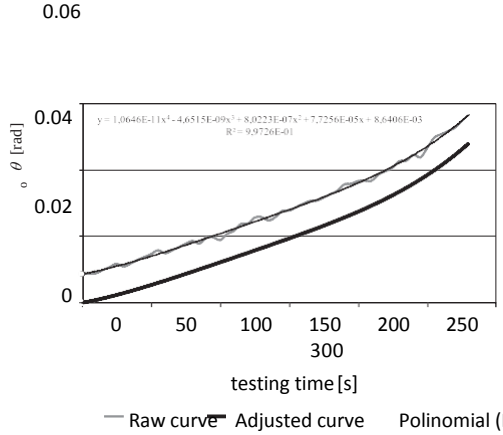

5. In fact, for h ¼ 1 mm, the value of G_{IC} ¼ 0.68870.153 N/mm was found. The improvement to the

Fig. 7. Plot of θ_O-testing time for a specimen with *h* ¼ 4 mm: raw curve, polynomial approximation and adjusted polynomial curve.

specimens with *h* ¼ 2 mm (considering average values) was of 13.8%, 48.3% to *h*¼3 mm and 56.7% to *h*¼4 mm.

4.2. Evaluation of G_{IC} by the J-integral

G_{IC} was calculated by Eq. (2), in which θ_O was estimated as described in Section 3.2.1.3 and plotted with the time elapsedsince the test initiation, with one data point every 5 s. Fig. 7 gives an example of the evolution of θ_O for a selected test specimen(with *h* ¼ 4 mm). This specimen is also used in the following figures as being representative of the tests. Shown in the graphicare the raw curve, the 4^{th} degree fitting curve and the corrected polynomial and final curve, adjusted to make θ_O(testing time¼0)¼0. It should be mentioned that the raw curve of eachspecimen was adjusted by the most suited polynomial functionbetween 3^{rd} and 6^{th} degrees, by choosing the best correlationfactor, *R* (this also applies to the forthcoming fitting data). This polynomial adjustment is required to smooth the raw data and
remove experimental measurement scatter, but also to cancel any eventual misalignment between glued scales in both adherends. The following step consisted on estimating the curve relating δ_n with the testing time, to determine the cohesive law by Eq. (5).

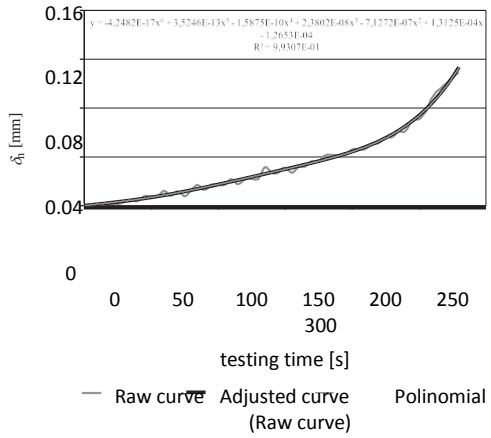

Fig. 8. Plot of δn-testing time for a specimen with h ¼ 4 mm: raw curve, polynomial approximation and adjusted polynomial curve.

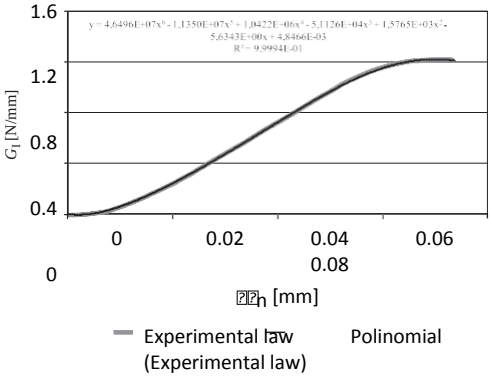

Fig. 9. Experimental Gn–δn law for one specimen and polynomial fitting.

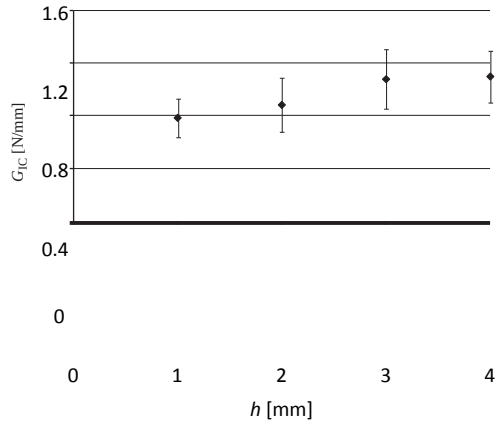

Fig. 10. Average values and deviation of GIC as a function of h by the J-integral.

Fig. 8 shows the δn-testing time plot for a specimen, more specifically the three curves of Fig. 7. Due to scaling difficulties, the raw curve in the figure is already translated such that δn(testing time¼ 0)¼ 0. GIC for each specimen was then defined
by the respective GI–δn curve, as the steady-state value of GI [17].
Fig. 9 follows the same specimen and shows the experimental GI– δn law and the corresponding 6th degree polynomial. This curveis representative of all specimens, and shows three regions: (1) slow increase of GI with δn, but with increasing growth rate of GI (up to δn ≤ 0.02 mm), (2) linear increase of GI (for this specimen between
0.02 mm ≤ δn ≤ 0.04 mm) and (3) gradual attainment of a steady- state value of GI (δn ≥ 0.075 mm). For this specimen, the measured

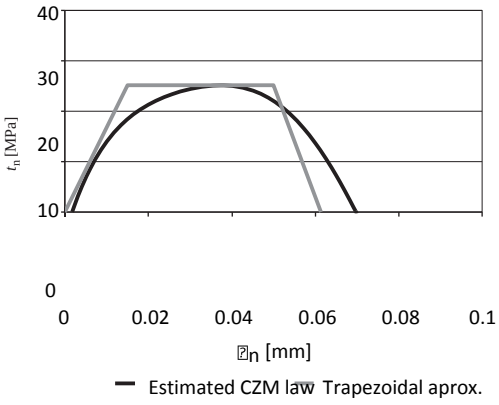

Fig. 11. Estimated tn–δn law for one test specimen and approximation.

in reference [40], where an average value of 1.182 N/mm was found in DCB specimens of natural fibre composites with h ¼ 5 mm. The tn–δn law for the test specimen followed in this section is presented in Fig. 11, together with a possible trapezoidal approximation, particularly suited to model CZM laws for ductile
adhesives [43]. The pertinent parameters for this specimen were t_n^0 ¼25.1 MPa and δnc¼0.0692 mm.

4.3. Discussion

The comparison between both of the proposed methods, the CBBM and J-integral, showed that under the present testing conditions both methods agree quite well, although the J-integralresults are slightly higher. Actually, the difference between average values was of 13.5%, 12.3%, 5.3% and 1.6% for increasing h values between 1 and 4 mm. Despite this small variation, which is probably due to statistical reasons, the observed trend was in high correlation, and in both cases a stabilization of GIC seems to occur at h ¼ 3 mm. At least, a much lesser effect exists from h ¼ 3 mm than for smaller values of h. This increase of GIC is reported in the literature because of the stress field variations ahead of the crack tip being dependent on the joint geometry,

value of GIC was 1.21 N/mm. The GIC results by applying this procedure for all tested specimens are shown in Fig. 10. The GIC evolution with h is consistent with that shown in Fig. 6. The deviation is larger, though, and whose justification lies on the experimental process to obtain GIC, which relies on a number of measured parameters and approximation functions, which are difficult to adjust to the experimental data [40]. While for the specimens with h ¼1 mm, a value of GIC ¼0.78170.146 N/mm was obtained, improvements of 12.6%, 37.7% and 40.2% were attained by increasing h up to 4 mm. These results reinforce the previous assumption on the stabilization of GIC for a given value of h (in this case of GIC ¼ 1.09570.195 N/mm for h ¼ 4 mm). This steady-state value of GIC can be compared with previous results by the authors

which highly influences the shape and size of the damage zone, and the local yield stress as well [44]. As it was discussed in previous works [45], thicker adherends provide an elevation of peel stresses further within the joint, shifting the loading condi- tions from peeling to cleavage, and giving a larger length for the damage zone. These findings are corroborated in the work of Azari et al. [46], regarding the adherend stiffness influence on the fatigue failure of bonded joints, which proved by finite elements that the plastic zone in adhesive joints between steel adherends was consistently higher than identical joints between aluminium adherends during the entire damage uptake process up to crack initiation. Pardoen et al. [23] developed an analytical model to study the constraint effects in adhesive joint fracture, considering steel adherends and two epoxy adhesives, and reported a sig- nificant increase of the adhesive plastic dissipation in the fully plastic regime by increasing the adherends thickness. The reported dependence of G_{IC} with h was also addressed in joints with composite adherends, in which h is defined by the number of plies, and results were found to be consistent with those of this work. Mangalgiri et al. [31] justified this tendency with the plastic zone and stress distributions ahead of the debond tip. Actually, the plastic zone was bigger in length across the adhesive layer with increasing number of composite plies (and thus, increasing h). Also, thicker adherends used a larger amount of the input energy to the specimen to develop a lengthier plastic zone, thus leaving less available energy for damage growth [47]. On account of this, higher values of G_{IC} can be expected for joints with higher degrees of restraint (i.e., stiffer or thicker adherends). On the other hand, because of the damage zone length limitation by the adhesive ductility, it is also noted that tough adhesives are particularly

prone to these effects, while brittle adhesives are not. The consideration of adherends with different stiffness provides a similar effect to the variation of h, as stiffer adherends give a higher restriction to the adhesive layer deformation. Under this scope, Bell and Kinloch [44] tested DCB specimens with alumi- nium, steel and carbon-fibre adherends, and obtained an increas- ing trend of G_{IC} with the adherend stiffness. Contradicting results were found by Choupani [48], but in this case the differences were given by a modification of the failure mechanism for the joints with stiffer adherends (steel compared to aluminium). With increasing values of h, eventually the plastic zone reaches a maximum, i.e., a value above which it does not increase any more, justifying the stabilization of G_{IC}. The plastic zone assumption implies that brittle adhesives are marginally affected, if so, by this parameter, and this was confirmed in the work of Fernlund and Spelt [49], whose results on DCB with aluminium adherends up to
12.7 mm thick and a brittle adhesive did not show any variations beyond the statistically related scatter.

5. Conclusions

This work aimed to analyse the influence of h on the measured value of G_{IC} of a ductile adhesive within a pure tensile test as it is the DCB test. Different values of h were considered, between 1 and 4 mm. Two techniques were used for G_{IC}, the CBBM and the J- integral. For the J-integral methodology, a relatively time-consuming approach was required, which involved evaluating by an optical method θ_O and δ_n at the crack tip during the test, followed by
polynomial fitting and differentiation. The trends between both methods were consistent, although the G_{IC} values obtained by the J-integral were slightly bigger than for the CBBM (between 1.6 and 13.5%, depending on h). Disregarding the data reduction method, an increasing trend of G_{IC} with h was found, suggesting that G_{IC} is not a material parameter, but a geometry-dependent quantity instead. The increase of G_{IC} was bigger for the smaller h values, eventually attaining a steady-state value for a given h value, as it sounded by comparing results for specimens with h¼3 and 4 mm. This result is highly relevant since structural bonding usually falls within small values of h, and was considered to be due to an increasing degree of adherend restraining for bigger h values, as a larger region is loaded ahead of the crack tip. The J-integral enabled obtaining the tensile CZM law of the adhesive. The CZM curves showed the large plasticity of the polyurethane adhesive. As output of this work, G_{IC} data was given for the strength prediction of bonded joints.

Acknowledgments

The authors would like to thank Sika^S for supplying the adhesive.

References

[1] da Silva LFM, Öchsner A, Adams RD, editors. Heidelberg: Springer; 2011.
[2] da Silva LFM, Campilho RDSG. Advances in numerical modelling of adhesive joints. Heidelberg: Springer; 2011.
[3] Campilho RDSG, Banea MD, Chaves FJP, da Silva LFM. eXtended finite element method for fracture characterization of adhesive joints in pure mode I. Comput Mater Sci 2011;50:1543–9.
[4] Volkersen O. Die nietkraftoerteilung in zubeanspruchten nietverbindungen konstanten loschonquerschnitten. Luftfahrtforschung 1938;15:41–7.
[5] Goland M, Reissner E. The stresses in cemented joints. J Appl Mech 1944;66:17–27.
[6] Hart-Smith LJ. Adhesive bonded single lap joints. NASA Contract Rep 1973;112235.
[7] Chai H. Shear fracture. Int J Fract 1988;37:137–59.
[8] Campilho RDSG, de Moura MFSF, Barreto AMJP, Morais JJL, Domingues JJMS. Fracture behaviour of damaged wood beams repaired with an adhesively- bonded composite patch. Composites Part A, 40; 2009; 852–9.
[9] Campilho RDSG, de Moura MFSF, Ramantani DA, Morais JJL, Domingues JJMS. Buckling behaviour of carbon-epoxy adhesively-bonded scarf repairs. J Adhes Sci Technol 2009;23:1493–513.
[10] Campilho RDSG, Banea MD, Neto JABP, da Silva LFM. Modelling of single-lap joints using cohesive zone models: effect of the cohesive parameters on the output of the simulations. J Adhes 2012;88:513–33.
[11] Yoshihara H. Simple estimation of critical stress intensity factors of wood by tests with double cantilever beam and three-point end-notched flexure. Holzforschung 2007;61:182–9.
[12] Wang SS. Fracture mechanics for delamination problems in composite materials. J Compos Mater 1983;17:210–23.
[13] de Moura MFSF, Campilho RDSG, Gonçalves JPM. Crack equivalent concept applied to the fracture characterization of bonded joints under pure mode I loading. Compos Sci Technol 2008;68:2224–30.
[14] Suo Z, Bao G, Fan B. Delamination R-curve phenomena due to damage. J MechPhys Solids 1992;40:1–16.
[15] Sorensen BF, Jacobsen TK. Characterizing delamination of fibre composites by mixed mode cohesive laws. Compos Sci Technol 2009;69:445–56.
[16] Zhu Y, Liechti KM, Ravi-Chandar K. Direct extraction of rate-dependent traction-separation laws for polyurea/steel interfaces. Int J Solids Struct 2009;46:31–51.
[17] Carlberger T, Stigh U. Influence of layer thickness on cohesive properties of an epoxy-based adhesive-an experimental study. J Adhes 2010;86:814–33.
[18] Ji G, Ouyang Z, Li G, Ibekwe S, Pang SS. Effects of adhesive thickness on global and local mode-I interfacial fracture of bonded joints. Int J Solids Struct. 2010;47:2445–58.
[19] Chen Z, Adams RD, da Silva LFM. Prediction of crack initiation and propagation of adhesive lap joints using an energy failure criterion. Eng Fract Mech 2011;78:990–1007.
[20] Kinloch AJ, Shaw SJ. A fracture mechanics approach to the failure of structural joints. In: Kinloch AJ, editor. Developments in adhesives—2. London: Applied Science Publishers; 1981. p. 83.
[21] da Silva LFM, de Magalhães FACRG, Chaves FJP, de Moura MFSF. Mode II fracture toughness of a brittle and a ductile adhesive as a function of the adhesive thickness. J Adhes 2010;86:891–905.
[22] Ashcroft IA, Shenoy V, Critchlow GW, Crocombe AD. A comparison of the prediction of fatigue damage and crack growth in adhesively bonded joints using fracture mechanics and damage mechanics progressive damage meth- ods. J Adhes 2010;86:1203–30.
[23] Pardoen T, Ferracin T, Landis CM, Delannay F. Constraint effects in adhesive joint fracture. J Mech Phys Solids 2005;53:1951–83.
[24] Wang RX, Sinclair AN, Spelt JK. Strength of adhesive joints with adherend yielding: II. Peel experiments and failure criteria. J Adhes, 79; 2003; 49–66.
[25] Ikeda T, Yamashita A, Lee D, Miyazaki N. Failure of a ductile adhesive layer constrained by hard adherends. J Eng Mater Technol 2000;122:80–5.
[26] Giannis S, Adams RD, Clark LJ, Taylor MA. The use of a modified peel specimen to assess the peel resistance of aircraft fuel tank sealants. Int J Adhes Adhes 2008;28:158–75.
[27] Ferracin T, Landis CM, Delannay F, Pardoen T. On the determination of the cohesive zone properties of an adhesive layer from the analysis of the wedge peel test. Int J Solids Struct 2003;40:2889–904.
[28] da Silva LFM, Carbas RJC, Critchlow GW, Figueiredo MAV, Brown K. Effect of material, geometry, surface treatment and environment on the shear strength of single lap joints. Int J Adhes Adhes 2009;29:621–32.
[29] Keller T, Vallée T. Adhesively bonded lap joints from pultruded GFRP profiles. PartI: Stress–strain analysis and failure modes. Composites Part B 2005;36:331–40.
[30] Pinto AMG, Campilho RDSG, Mendes IR, APM Baptista. Numerical and experimental analysis of balanced and unbalanced adhesive single-lap joints between aluminium adherends, J Adhes. doi: 10.1080/00218464.2013.773258.

[31] Mangalgiri PD, Johnson WS, Everett Jr RA. Effect of adherend thickness and mixed mode loading on debond growth in adhesively bonded composite joints. J Adhes 1987;23:263–88.
[32] Devitt DF, Schaperv RA, Bradley WL. A method for determining the mode I delamination fracture toughness of elastic and viscoelastic composite materi- als. J Compos Mater 1980;14:270–85.
[33] Campilho RDSG, Banea MD, Pinto AMG, da Silva LFM, de Jesus AMP. Strength prediction of single-and double-lap joints by standard and extended finite element modelling. Int J Adhes Adhes 2011;31:363–72.
[34] Pinto AMG, Campilho RDSG, Mendes IR, Aires SM, Baptista APM. Effect of hole drilling at the overlap on the strength of single-lap joints. Int J Adhes Adhes 2011;31:380–7.
[35] Neto JABP, Campilho RDSG, da Silva LFM. Parametric study of adhesive joints with composites. Int J Adhes Adhes 2012;37:96–101.
[36] Giovanola JH, Finnie I. A review of the use of the *J* integral as a fracture parameter. Solid Mech Arch 1984;9:197–225.
[37] Banea MD, da Silva LFM, Campilho RDSG. Effect of temperature on tensile strength and mode I fracture toughness of a high temperature epoxy adhesive. J Adhes Sci Technol 2012;26:939–53.
[38] Rice JR. A path independent integral and the approximate analysis of strain concentration by notches and cracks. J Appl Mech 1968;35:379–86.
[39] Banea MD, da Silva LFM, Campilho RDSG. Temperature dependence of the fracture toughness of adhesively bonded joints. J Adhes SciTechnol 2010;24:2011–26.
[40] Campilho RDSG, Moura DC, Gonçalves DJS, da Silva JFMG, Banea MD, da Silva LFM. Fracture toughness determination of adhesive and co-cured joints in natural fibre composites. Composites Part B 2013;50:120–6.

[41] Lewis JP. Fast template matching, vision interface 95, Canadian Image Processing and Pattern Recognition Society, Quebec City, Canada, May 15-19, 1995, p. 120–123.

[42] Zhang Z. Camera calibration. In: Emerging topics in computer vision, G Medioni S Kang, editors. Prentice Hall Professional Technical Reference, 2004, ch. 2.

[43] Campilho RDSG, de Moura MFSF, Barreto AMJP, Morais JJL, Domingues JJMS. Experimental and numerical evaluation of composite repairs on wood beams damaged by cross-graining. Constr Build Mater 2010;24:531–7.

[44] Bell AJ, Kinloch AJ. The effect of the substrate material on the value of the adhesive fracture energy, *Gc*, J. Mater Sci Lett 1997;16:1450–3.

[45] Blackman BRK, Kinloch AJ, Paraschi M. The effect of the substrate material on the value of the adhesive fracture energy, *Gc*: further considerations. J Mater Sci Lett 2001;20:265–7.

[46] Azari S, Ameli A, Datla NV, Papini M, Spelt JK. Effect of substrate modulus on the fatigue behaviour of adhesively bonded joints. Mater Sci Eng, A 2012;534:594–602.

[47] Azari S, Ameli A, Papini M, Spelt JK. Adherend thickness influence on fatigue behaviour and fatigue failure prediction of adhesively bonded joints. Compo- sites Part A 2013;48:181–91.

[48] Choupani N. Mixed-mode cohesive fracture of adhesive joints: experimental and numerical studies. Eng Fract Mech 2008;75:4363–82.

[49] Fernlund G, Spelt JK. Mixed-mode fracture characterization of adhesive joints. Compos Sci Technol 1994;54:441–9.